Biochimica et Biophysica Acta 1818 (2012) 2884–2891

Contents lists available at SciVerse ScienceDirect

Biochimica et Biophysica Acta

journal homepage: www.elsevier.com/locate/bbamem

Structure of solid-supported lipid membrane probed by noble metal nanoparticle deposition

Hyeun Hwan An, Seung Jae Lee, Hee-Soo Kim, Won Bae Han, Chong Seung Yoon *

Division of Materials Science and Engineering, Hanyang University, Seoul, 133-791, Republic of Korea

ARTICLE INFO

Article history:
Received 9 April 2012
Received in revised form 4 July 2012
Accepted 11 July 2012
Available online 20 July 2012

Keywords:
Lipid membrane
Nanoparticle
Phase transition

ABSTRACT

Direct deposition of a noble metal layer onto a solid-supported membrane was proposed as an indirect microscopy tool to visually observe different lipid phases that may develop in the lipid membrane. The method relied on the different permeability of the lipid membrane towards the incident atoms during deposition. Liquid state or structural defects such as phase boundaries, step ledges in a multi-lamellar stack, and pores permitted the metal atoms to penetrate and nucleate inside the membrane whereas rigid gel state was relatively impermeable to the incident atoms, thus enabling visualization of liquid phase or structural defects inside the gel state. Based on the proposed method, we demonstrated the phase states resulting from thermotropic transitions of 1,2-dipalmitoyl-sn-glycero-3-phosphocholine (DPPC), dioleoylphosphatidylethanolamine (DOPE)/DPPC mixture, and 1,2-dioleoyl-3-trimethylammonium propane (DOTAP). Although the proposed method does not allow in-situ observation of equilibrium states, the method should be an excellent complementary tool for visualizing the lipid phases as the method can resolve fine structural details (up to tens of nanometer scale) as seen in the DPPC membrane while providing macroscopic images (up to several micrometers).

1. Introduction

A solid-supported lipid membrane has been traditionally used to simulate the molecular processes occurring at the biological membranes [1]. With recent developments in nanotechnology and sophisticated analytical tools, potential application of solid-supported lipid membranes has greatly expanded to biomedical materials and biofunctional devices [2]. In fact, solid-supported lipid membranes were used to demonstrate the electrical bistability of organic memory nanodevice [3] and develop a voltametric sensor [4,5] and multilayer grating [6] for biosensing. Solid-supported lipid membranes were also used as a template to fabricate nanostructured materials [7]. Previously, noble metal (Ag and Au) and transition metal oxide nanoparticles were produced by direct deposition of the respective metal onto a supported lipid membrane [8]. During the process, it was found that depending on the lipid phase the interaction of the metal atoms with the lipid membrane was dramatically different. A lipid membrane in its liquid state, L_α was permeable to the incident metal atoms, thus allowing the metal atoms to penetrate the membrane surface and to form metal nanoparticles below the membrane surface whereas in the rigid gel state, L_β the incident metal atoms were unable to penetrate and nucleate inside the lipid membrane. In this paper, we propose a simple method of studying the phase state of lipid molecules based on the observed difference in the metal interaction with the solid-supported lipid membrane. Phase states of lipids are usually determined using nuclear magnetic resonance [9], small angle X-ray scattering [10], and differential scanning calorimetry [11] but these methods are macroscopic and do not provide local spatial information. Confocal fluorescent microscopy (CFM) can supply mesoscopic spatial information, but its resolution is still limited to a micrometer scale [12]. Meanwhile, atomic force microscopy (AFM) is the preferred tool to elicit local structural information of various lipid systems with the highest spatial resolution [13]. Because AFM is inherently surface-sensitive, obtaining clean AFM images is not always trivial. On the other hand, the phase state of lipids between liquid and gel states can be routinely detected by the deposition of noble metal onto the lipid membrane and transmission electron microscopy (TEM). In addition, the morphology and arrangement of nanoparticles can provide a great deal of information on the local structure of the lipid membrane because the nanoparticles formed inside the membrane range are in a nanometer scale in size. The proposed method would be an excellent complementary microscopy tool to probe the structural changes in the lipid membrane in addition to AFM and CFM. 1,2-dipalmitoyl-*sn*-glycero-3-phosphocholine (DPPC) whose main gel-to-liquid crystalline phase transition ($L_\beta \rightarrow L_\alpha$) occurs at ~40 °C in excess water [14] was employed to demonstrate the potential use of the proposed method. In addition, previously unreported high-temperature phase transition of 1,2-dioleoyl-3-trimethylammonium propane (DOTAP) and immiscibility of DPPC with dioleoylphosphatidylethanolamine (DOPE) are also included to further ascertain the reliability of the method to probe the phases of different lipid systems.

* Corresponding author. Fax: +82 2 2220 1838.
E-mail address: csyoon@hanyang.ac.kr (C.S. Yoon).

0005-2736/$ – see front matter © 2012 Elsevier B.V. All rights reserved.
doi:10.1016/j.bbamem.2012.07.006

2. Materials and methods

Solid-supported lipid membranes were prepared by spin-coating the lipid solution onto a Si substrate. Lipid solution was made by dissolving the lipids (DPPC, DOPE, and DOTAP purchased from Avanti Polar Lipids Inc.) in chloroform (10 mg/ml). 100 μl of the lipid solution was used to form the multilayer by spin coating the lipid solution at 5000 rpm onto a 2 cm×2 cm Si substrate. After spin coating, the solvent was allowed to evaporate in a freeze dryer for 12 h. The solid-supported lipid membranes were immediately placed into a humidity-controlled furnace which was pre-conditioned to the desired humidity and temperature for 2 h prior to each experiment to minimize the effect of heating/cooling rates on the lipid phase transition. The lipid membrane was kept at different temperatures (10 °C–60 °C) at 80% relative humidity (RH) for 24 h in the furnace. To probe the phase state of the lipid membranes, the conditioned membrane was immediately removed from the furnace and transferred into a vacuum chamber for metal evaporation. In order to reach the desired vacuum level, the chamber was pumped for 3 h prior to the metal evaporation. Then 3-nm-thick Ag (or Au) layer was deposited using a thermal evaporator. The amount of Ag (or Au) was monitored using a quartz balance. The sample was shielded from the metal source using a shutter (as heat transfer occurs mainly by radiation in the vacuum chamber) and the sample was exposed to the source for 1.5 min for the metal deposition (deposition rate of 0.01 nm/s). TEM (JEOL 2010) was used to characterize the Ag (or Au) nanoparticle morphology. For preparing the TEM specimen, a TEM Cu grid covered with amorphous carbon film was placed on the substrate prior to the lipid spin-coating. The lipid spin-coating, annealing and metal deposition were carried out directly on the TEM grid. TEM observation was made without further treatment of the specimen. In order to ensure that the phase state of the lipid membrane was not affected by the metal deposition, AFM measurements were carried on the treated membranes before the metal deposition to corroborate the TEM results.

3. Results and discussion

DPPC undergoes sub-, pre-, and main transitions during which subgel phase, $L_{c'}$ changes to L_{β} at 19 °C, L_{β} to ripple phase, $P_{\beta'}$ at 36.5 °C and finally $P_{\beta'}$ to L_{α} at 41.9 °C [15]. In order to observe the structure of the DPPC membrane at different phase states, the DPPC membrane heated to different temperatures up to 60 °C was cooled to room temperature for the metal deposition; hence, it is noted that the DPPC membrane was not in its equilibrium state when observed by TEM; therefore, it was not able to observe all the phases developed during the $L_{\beta} \rightarrow L_{\alpha}$ transition.

Fig. 1 shows a set of TEM images from the DPPC membrane that was kept at 10 °C and 80% RH for 24 h after which 3-nm-thick Ag was deposited on the membrane. From the low magnification TEM image in Fig. 1(a), it appears that the DPPC membrane which should be in its gel state has a series of flat terraces with sharp steps. The TEM image closely resembles the steps observed in the multi-lamellar stacks of DPPC in the gel state prior to the main transition, imaged by AFM [16].

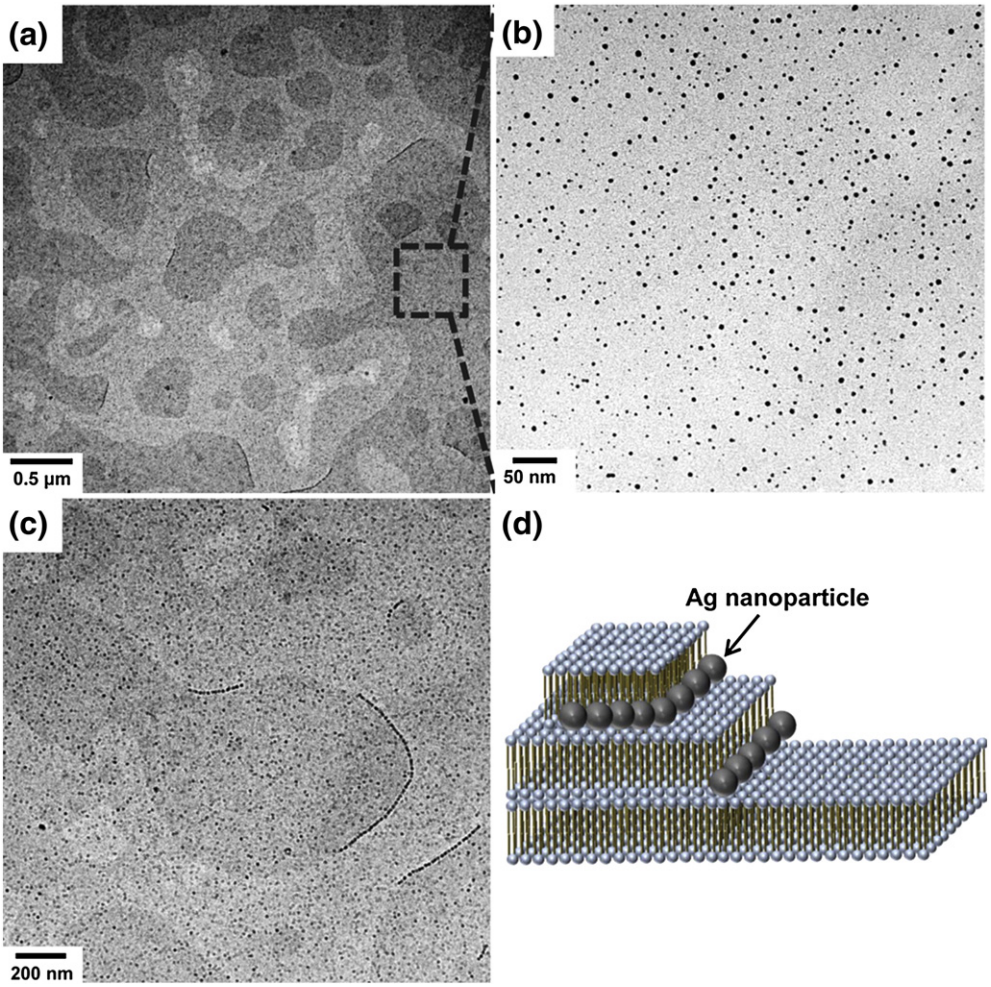

Fig. 1. TEM images of the Ag nanoparticles from the DPPC membrane that were kept at 10 °C and 80% RH for 24 h after which 3-nm-thick Ag was deposited on the membrane at room temperature, (d) schematic image the Ag nanoparticles nucleated on the lipid stack ledges.

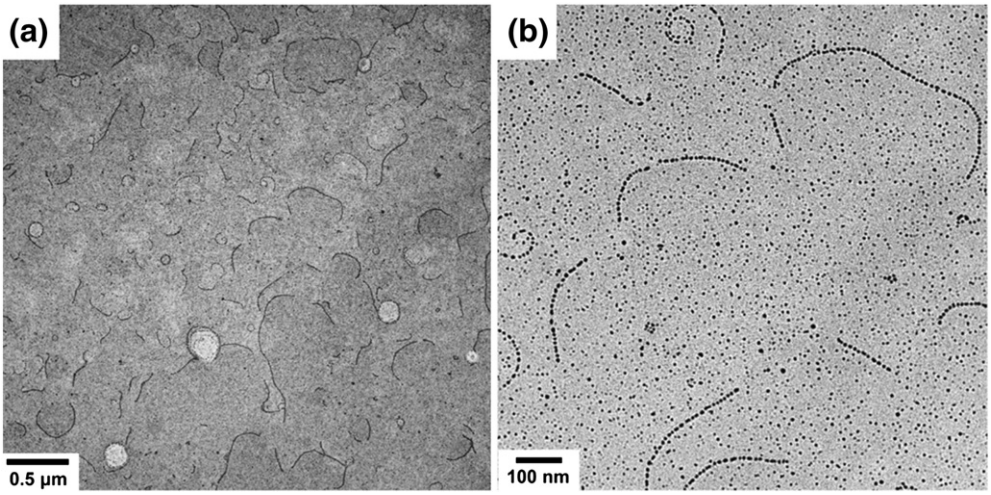

Fig. 2. TEM images of the Ag nanoparticles from the DPPC membrane that were kept at 20 °C and 80% RH for 24 h after which 3-nm-thick Ag was deposited on the membrane at room temperature.

The Ag nanoparticles formed inside the DPPC membrane can be seen in a magnified TEM image in Fig. 1(b). The Ag nanoparticles whose average diameter was 3.2 ± 0.8 nm were sparsely distributed. The DPPC membrane in the gel state is stiffer compared to the liquid crystalline membrane, which was attested by force spectroscopy using AFM so that it took a greater force for the AFM tip to penetrate or puncture the gel phase than the liquid phase [17]. Hence, the incident Ag atoms were hardly able to penetrate the DPPC membrane and nucleate inside the gel membrane. In the case of the liquid state, it was amply demonstrated that Ag atoms formed a dense monolayer of nanoparticles within the membrane [7]. Example in which a string of Ag nanoparticles was formed along the terrace (or lamellar) step is shown in Fig. 1(c). Even though the Ag atoms could not nucleate inside the gel membrane, a string or cluster of Ag nanoparticles were found along defects such as surface steps as Fig. 1(c) or domain boundaries as schematically illustrated in Fig. 1(d).

At 20 °C, judging from the uniform contrast of the TEM image in Fig. 2(a), the membrane became considerably flat and numerous linear strings of Ag nanoparticles were observed as shown in Fig. 2(b). The strings of Ag nanoparticles appeared to occupy the boundary between two domains that were used to be at different heights since the areas approximately enclosed by the Ag nanoparticle strings were close to those of the dark regions in Fig. 1(a). Narrow cracks in the bilayer surface of DPPC have been previously observed by AFM [18,19] and was preferentially filled by C14-peptide molecules [19], similar to the Ag nanoparticles shown in Fig. 2(b).

For the sample that had been kept at 30 °C which was close to the $L_{\beta} \rightarrow P_{\beta'}$ pretransition temperature, there were numerous small circular regions completely enclosed by the Ag nanoparticles while accompanied by the disappearance of the strings of nanoparticles related to the defect lines as shown in Fig. 3(a). The enclosed loops were ~50 nm in diameter. A magnified image in Fig. 3(b) demonstrates the difference in size and packing of the Ag nanoparticles inside and outside the enclosed region. The Ag nanoparticles inside the enclosed loop were much smaller in size compared to the nanoparticles outside, but densely packed. The dense packing of the nanoparticles inside the enclosed areas suggests that the circular region is likely in a fluid-like state. Although coexistence of the metastable $L_{\alpha} + L_{\beta}$ region before the transition to $P_{\beta'}$ during rapid cooling of a binary lipid system has been suggested [20,21], to our best knowledge, an intermediate fluid state prior to the $L_{\beta} \rightarrow P_{\beta'}$ transition for DPPC has not been reported. Considering the fact that the membrane was in a non-equilibrium state,

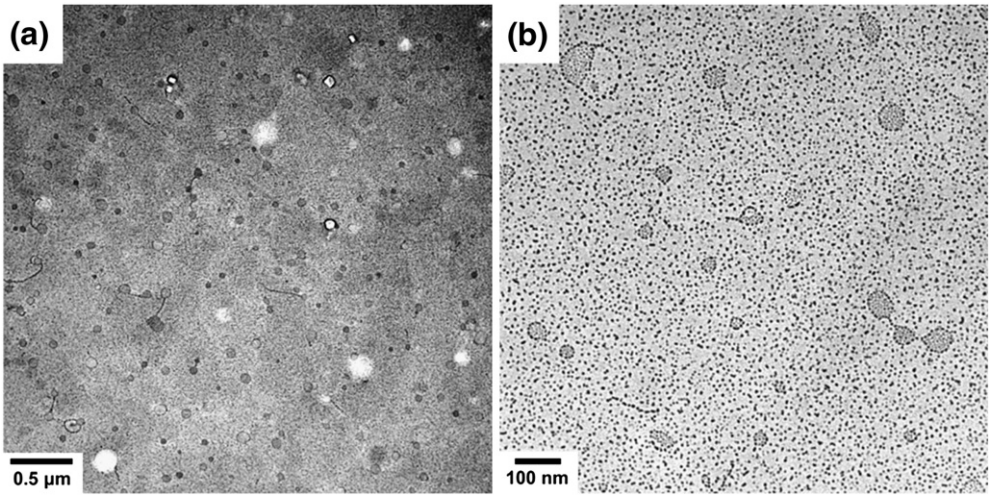

Fig. 3. TEM images of the Ag nanoparticles from the DPPC membrane that were kept at 30 °C and 80% RH for 24 h after which 3-nm-thick Ag was deposited on the membrane at room temperature.

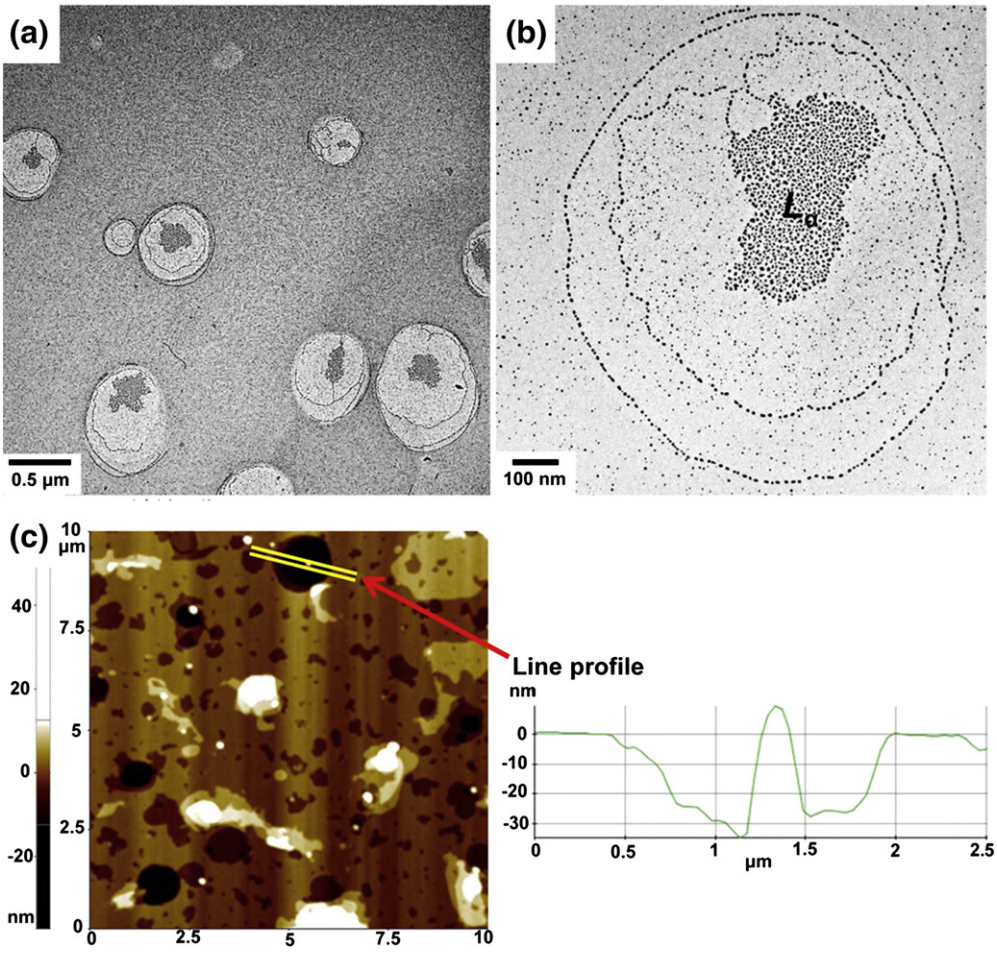

Fig. 4. (a), (b) TEM images of the Ag nanoparticles from the DPPC membrane that were kept at 40 °C and 80% RH for 24 h after which 3-nm-thick Ag was deposited on the membrane at room temperature, (c) AFM image of the DPPC membrane prior to the Ag deposition together with the depth profile along the marked line.

it is speculated that the enclosed loops may be cluster of point defects which would be re-arranged into a linear structure for the formation of $P_{\beta'}$ [22].

After heating to 40 °C just below the main transition, there were large areas in the membrane whose boundary was distinctively marked by encircling Ag nanoparticles as shown in Fig. 4(a). The encircled region was lighter in color, and a core with a higher density of Ag nanoparticles was observed at the center of the enclosed region. In fact, the monolayer of densely packed Ag nanoparticles in the core well matched the morphology of the Ag nanoparticles embedded in the L_α state. Since AFM images of $P_{\beta'}$ and L_α phases have been simultaneously observed well below the main transition [21,23], the enclosed region outside the L_α region may be a remnant ripple phase left over during cooling from 40 °C to room temperature. The

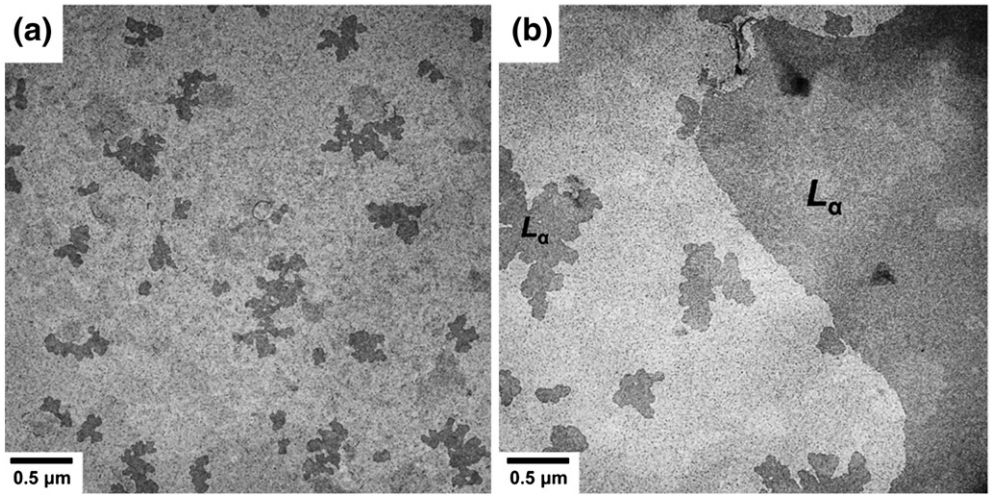

Fig. 5. TEM images of the Ag nanoparticles from the DPPC membrane that were kept at 50 °C and 80% RH for 24 h after which 3-nm-thick Ag was deposited on the membrane at room temperature.

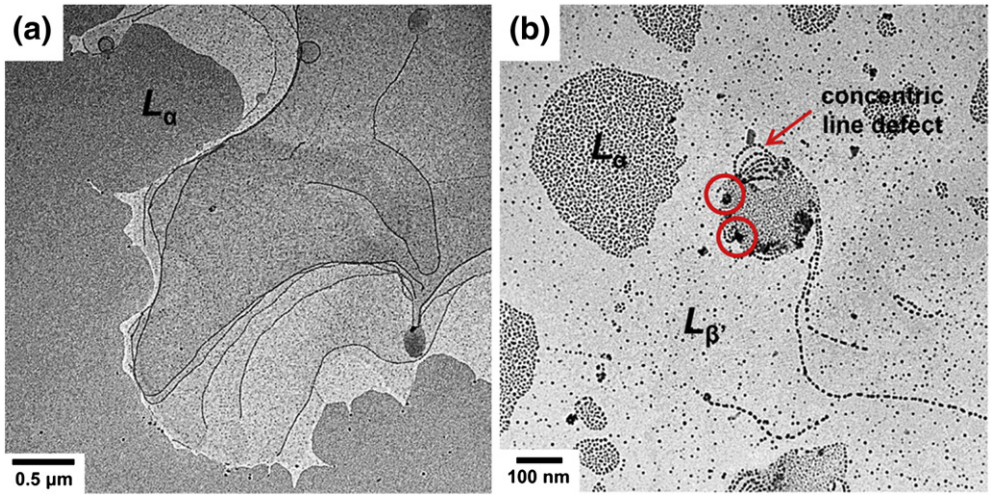

Fig. 6. (a) TEM images of the Ag nanoparticles from the DPPC membrane that were kept at 60 °C and 80% RH for 24 h after which 3-nm-thick Ag was deposited on the membrane at room temperature. Circles in (b) indicate the agglomerated Ag nanoparticles in the voids in the membrane.

Ag nanoparticles demarcating the phase boundary exhibited facets that may have developed due to the presence of a ripple phase whose presence can only be speculated by the proposed method. Meanwhile, the surrounding bulk returned to the equilibrium gel phase. An AFM image of the same sample prior to the Ag deposition shown in Fig. 4(c) reproduced general structural features observed using TEM with large circular regions with peaks in the center. However, we could not confirm the ripple phase at the phase boundary with AFM. However, the similarity between the AFM image in Fig. 4(c) and the image obtained using TEM at least affirms that the

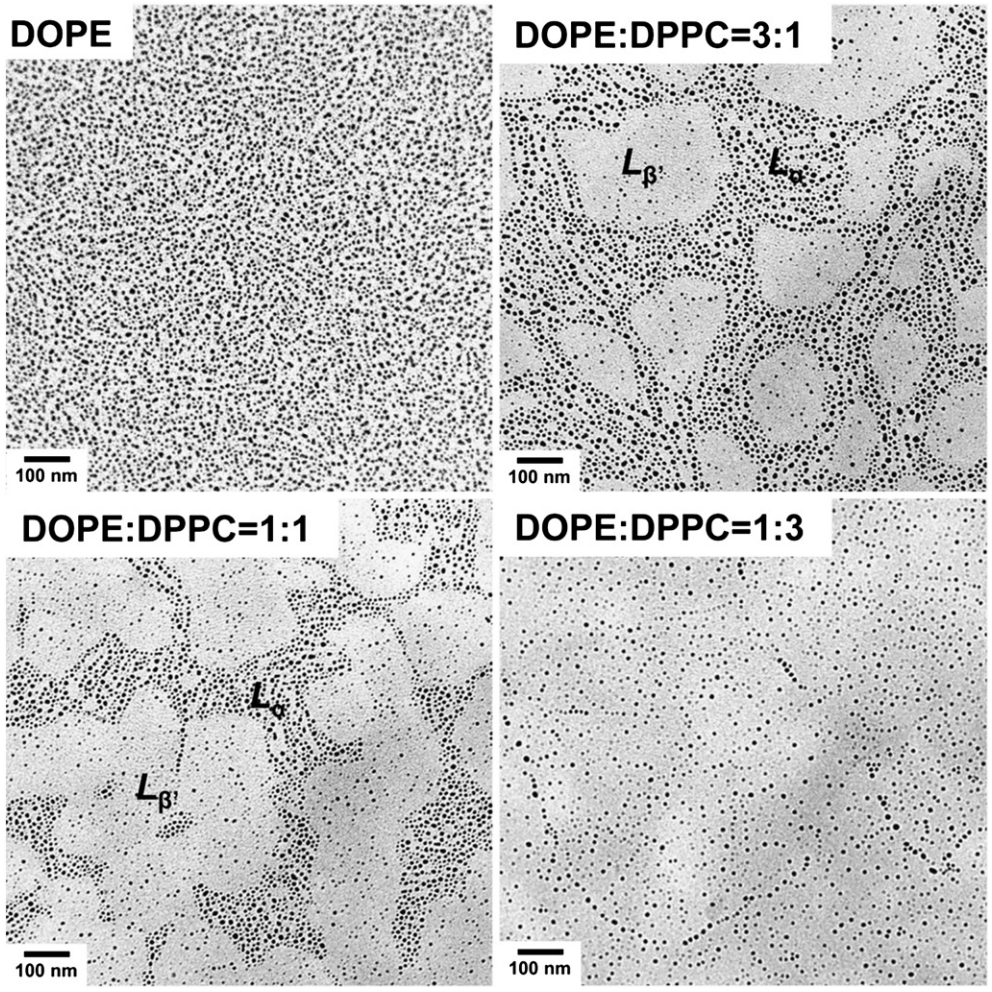

Fig. 7. TEM images of the Ag nanoparticles formed in the DPPC/DOPC mixture membrane at different ratios.

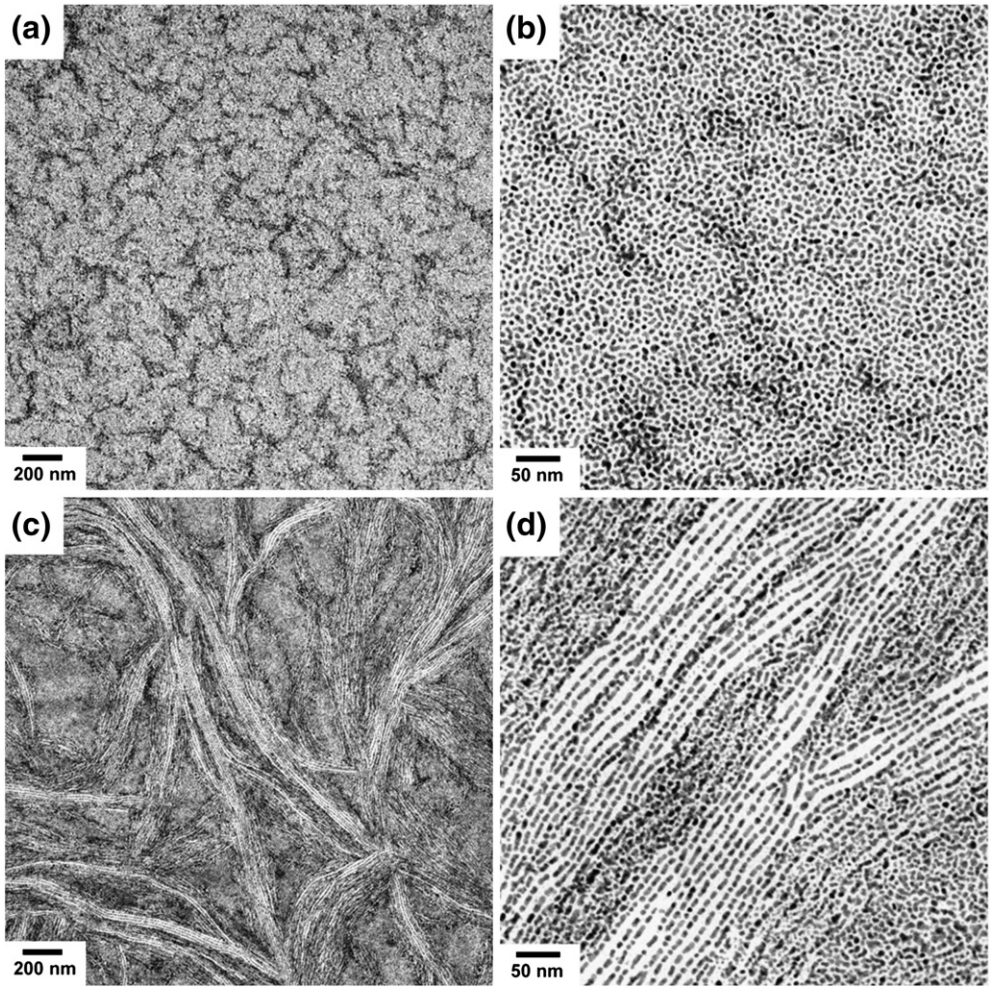

Fig. 8. TEM images of Au nanoparticles deposited onto the DOTAP membrane that were heat treated (a), (b) at 50 °C and (c), (d) at 80 °C with 50% RH prior to the metal deposition.

TEM images shown in Fig. 4 were not artifacts produced by the interaction of metal nanoparticles with the membrane. In fact, direct correspondence between the TEM and AFM images was also observed at other temperatures which are shown in Fig. S1–S6 in the Supporting Material. Therefore, the TEM image in Fig. 4 could represent an incipient stage of the main transition.

At 50 °C well above the main transition temperature, densely packed Ag nanoparticles indicative of the liquid state were uniformly distributed throughout most of the DPPC membrane. Fig. 5(a) shows an occasional region that remained untransformed with large isolated islands of L_α arrested in L_β. The sharp phase boundary demarcating L_α from L_β that is shown in Fig. 5(b) clearly differentiates the two phases with relatively larger Ag nanoparticles with higher number of particles per unit area observed in the L_α side. The DPPC membrane cooled from 60 °C in Fig. 6(a) is similar to those previously produced using in-situ AFM during the main phase transition [24]. The L_α region is flat with uniform contrast whereas the L_β region had multiple stacks with the stack boundary mapped out by the Ag nanoparticles. Shown in Fig. 6(b) is an area with complex defect structures. The region contained islands of L_α and the unidentified intermediate phase as seen in Fig. 3(b) inside the L_β matrix. Agglomeration of Ag nanoparticles (marked in Fig. 6(b) by circles) possibly produced by voids in the membrane was also observed. In addition, nearly concentric lines of defects emanating from the enclosed region in the center were also observed. Fig. 6(b) exemplify some of the structural details that can be revealed using the proposed method.

A series of TEM images in Fig. 7 further illustrates the capability of the proposed method to distinguish L_α or H_{II} from L_β. DPPC was mixed with DOPE whose gel-to-liquid transition is below 0 °C [25]. Because two lipids are immiscible at room temperature due to the large difference in the main transition temperature, phase separation occurs in the two-component membrane [26]. Fig. 7 clearly shows the change in the Ag nanoparticles density depending on the lipid phase as observed in the case of the DPPC phase transition in Fig. 5. Increasing fraction of L_β and H_{II} (or L_α and H_{II} mixture) with increasing DOPE concentration can be easily recognized from Fig. 7.

Furthermore, the lipid phase identification that can be made with the proposed is not limited to L_α and L_β. TEM images of Au nanoparticles deposited onto the DOTAP membrane that had been heat treated at 50 °C and 80 °C with 50% RH prior to the metal deposition is shown in Fig. 8. DOTAP's gel-to-liquid transition is at 0 °C [27] and should remain as L_α above the room temperature. A TEM image of the Au nanoparticles formed inside the DOTAP membrane that has been heat treated at 50 °C is shown in Fig. 8(a). Similar to the case of the DPPC membrane in L_α, the Au nanoparticles were densely packed with areas where the Au nanoparticles stacked on top of one another. A magnified image in Fig. 8(b) shows that the Au nanoparticles were uniformly distributed with no obvious pattern. However, after heating the DOTAP membrane to 80 °C, the Au nanoparticle deposition in Fig. 8(c) revealed a complex structure that was strikingly different from that obtained after heating the DOTAP membrane to 50 °C. A series of distinctive parallel strings of Au nanoparticles was observed. A magnified TEM image in Fig. 8(d)

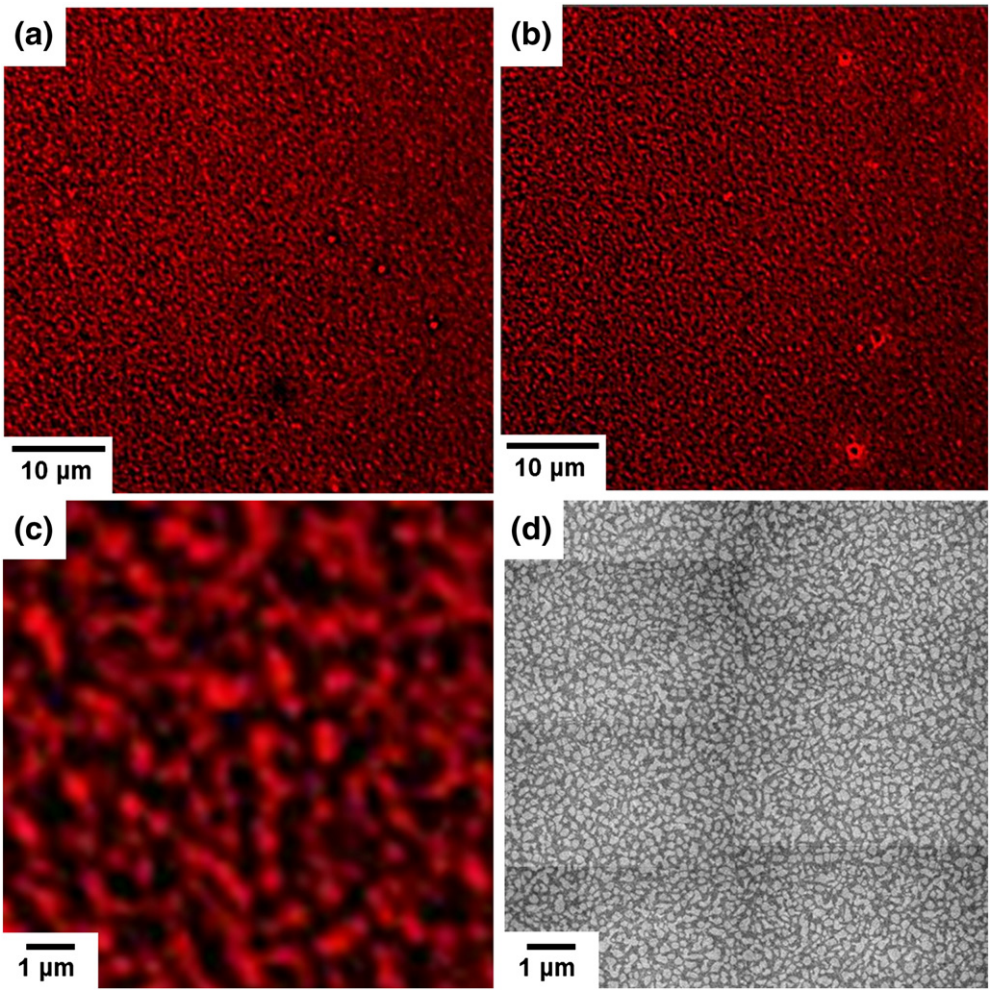

Fig. 9. Fluorescence microscopy images from the mixture of DOPE and DPPC in 1:1 ratio taken using Texas Red® 1,2-dihexadecanoyl-*sn*-glycero-3-phosphoethanolamine (a) before and (b) after Ag metal deposition, (c) magnified fluorescence microscopy image of (b) after the metal deposition, (d) composite TEM image of the same sample.

shows the linear alignment of the Au nanoparticles and the shapes of the Au nanoparticles that were elongated along the direction of the particle alignment into a cylindrical form. The TEM images in Fig. 8(c) and (d) were comparable to the Au nanoparticles previously found in a pure DOPE membrane. DOPE can exist in an inverted hexagonal phase, H_{II} at room temperature when hydrated [28]. We have previously demonstrated that a linear alignment of Ag nanoparticles can be generated in a solid-supported DOPE membrane by hydration and concluded that the linear arrangement was produced by the Ag nanoparticles selectively occupying the inter-channel pores [29]. It is speculated that DOTAP molecules undergo a phase transition from L_{α} to a three-dimensional phase such as H_{II} at an elevated temperature although such phase transition of DOTAP has not been reported in the literature. The phase transition may not be relevant because of the high temperature (~70 °C as can be seen from the TEM images of the Au nanoparticles deposited after annealing at 30 °C and 70 °C in Fig. S7 in the Supporting Material) at which the phase transition occurs, Fig. 8 visually demonstrates an existence of a high-temperature ordered phase for DOTAP and the capability of the proposed to recognize such a phase.

Lastly, in order to demonstrate the reliability of the proposed method, fluorescence microscopy images of the mixture of DOPE and DPPC in 1:1 ratio was obtained using Texas Red® 1,2-dihexadecanoyl-*sn*-glycero-3-phosphoethanolamine (0.1 mol%). Two fluorescence microscopy images in Fig. 9(a) and (b) taken before and after Ag metal deposition confirm that the metal nanoparticle deposition did not perturb the morphology of the lipid membrane at least at the micro-meter scale as the two images were nearly identical. Fig. 9(c) and (d) compares the fluorescence microscopy image after the metal deposition with the TEM image taken from the same sample. The TEM image is a mosaic composite image of 8 different TEM images to display the two images in Fig. 9(c) and (d) on the same scale. Because of the limitation in the resolution of fluorescence microscopy, it was difficult to exactly correlate the fluorescent image with the image obtained by electron microscopy. However, the general features shown in the fluorescence microscopy images (grainy appearance) were reproduced with much detail in the low magnification TEM image in Fig. 9(d). Fig. 9 thus verifies that the proposed microscopy method can faithfully reproduce structural details of lipid membrane systems with high resolution.

4. Conclusion

We have proposed an indirect microscopy tool to visually observe different lipid phases that may develop in a solid-supported lipid membrane. The method relied on the different permeability of the lipid membrane towards the incident atoms during deposition of noble metal layer on the lipid membrane. Liquid state or structural defects such as phase boundaries, step ledges in a multi-lamellar stack, and pores permitted the metal atoms to penetrate and nucleate inside the membrane, thus enabling the visualization of such structures. Based on the proposed method, we demonstrated the phase states resulting from thermotropic transitions of DPPC, DOPE/DPPC mixture, and DOTAP. Although the proposed method does not allow in-situ observation of equilibrium states, the method should be an

excellent complementary tool for visualizing the lipid phases as the method can resolve fine structural details (up to tens of nanometer scale) as seen in the DPPC membrane while providing macroscopic images (up to several micrometers).

Acknowledgement

This work was supported by the National Research Foundation of Korea (NRF) grant funded by the Korean government (MEST) (No. 2012000815).

Appendix A. Supplementary data

Supplementary data to this article can be found online at http://dx.doi.org/10.1016/j.bbamem.2012.07.006.

References

[1] R.P. Richter, R. Berat, A.R. Brisson, Formation of solid-supported lipid bilayers: an integrated view, Langmuir 22 (2006) 3497–3505.
[2] R.P. Richter, J.L.K. Him, A. Brisson, Supported lipid membranes, Mater. Today 6 (2003) 32–37.
[3] B. Yuan, S. Hu, N. Lu, F. Xu, K. Zhou, Y. Ma, M. Li, Electrical bistability in self-assembled hybrid multilayers of phospholipid and nanoparticles, Nanotechnology 22 (2011) 315303.
[4] P. Alessio, F.J. Pavinatto, O.N. Oliveira Jr., J.A.D.S. Saez, C.J.L. Constantino, M.L. Rodriguez-Mendez, Detection of catechol using mixed Langmuir–Blodgett films of a phospholipid and phthalocyanines as voltammetric sensors, Analyst 135 (2010) 2591–2599.
[5] C. Ge, K.S. Orosz, N.R. Armstrong, S.S. Saavedra, Poly(aniline) nanowires in sol gel coated ITO: a pH-responsive substrate for planar supported lipid bilayers, Appl. Mater. Interfaces 3 (2011) 2677–2685.
[6] S. Lenhert, F. Brinkmann, T. Laue, S. Walheim, C. Vannahme, S. Klinkhammer, M. Xu, S. Sekula, T. Mappes, T. Schimmel, H. Fuchs, Lipid multilayer gratings, Nat. Nanotechnol. 5 (2010) 275–279.
[7] N. Oh, J.H. Kim, C.S. Yoon, Self-assembly of silver nanoparticles synthesized by using a liquid-crystalline phospholipid membrane, Adv. Mater. 20 (2008) 3404–3409.
[8] H.H. An, J.H. Kim, J.H. Lee, D.H. Kwon, H. Kim, Y.H. Kim, C.S. Yoon, Interaction of a solid supported liquid-crystalline phospholipid membrane with physical vapor deposited metal atoms, Chem. Commun. 46 (2010) 9238–9240.
[9] K. Gawrisch, V.A. Parsegian, D.A. Hajduk, M.W. Tate, S.M. Gruner, N.L. Fuller, R.P. Rand, Energetics of a hexagonal-lamellar-hexagonal-phase transition sequence in dioleoylphosphatidyl-ethanolamine membranes, Biochemistry 31 (1992) 2856–2864.
[10] I. Koltover, T. Salditt, J.O. Radler, C.R. Safinya, An inverted hexagonal phase of cationic liposome–DNA complexes related to DNA release and delivery, Science 281 (1998) 78–81.
[11] C. Naumann, T. Brumm, T.M. Bayerl, Phase transition behavior of single phosphatidylcholine bilayers on a solid spherical support studied by DSC, NMR and FT-IR, Biophys. J. 63 (1992) 1314–1319.
[12] J.B. Pawley, In: Handbook of Biological Confocal Microscopy, third edition, SpringerScience+Business Media, New York, 2006, pp. 20–42.
[13] T. Fukuma, M.J. Higgins, S.P. Jarvis, Direct imaging of lipid-ion network formation under physiological conditions by frequency modulation atomic force microscopy, Phys. Rev. Lett. 98 (2007) 106101.
[14] S. Mabrey, J.M. Sturtevant, Investigation of phase transitions of lipids and lipid mixtures by high sensitivity differential scanning calorimetry, Biochemistry 73 (1976) 3862–3866.
[15] F. Wu, Q. Jia, R. Wu, Z.J. Yu, Regional cooperativity in the phase transitions of dipalmitoylphosphatidylcholine bilayers: the lipid tail triggers the isothermal crystallization process, Phys. Chem. B 115 (2011) 8559–8568.
[16] N. Maeda, T.J. Senden, J.D. Meglio, Micromanipulation of phospholipid bilayers by atomic force microscopy, Biochim. Biophys. Acta 1564 (2002) 165–172.
[17] S. Garcia-Manyes, G. Oncins, F. Sanz, Effect of temperature on the nanomechanics of lipid bilayers studied by force spectroscopy, Biophys. J. 89 (2005) 4261–4274.
[18] H.A. Rinia, R.A. Kik, R.A. Demel, M.M.E. Snel, J.A. Killian, J.P.J.M.V.D. Eerden, B.D. Kruijff, Visualization of highly ordered striated domains induced by transmembrane peptides in supported phosphatidylcholine bilayers, Biochemistry 39 (2005) 5852–5858.
[19] T.B. Pederson, T. Kaasgaard, M.O. Jensen, S. Frokjaer, O.G. Mouritsen, K. Jorgensen, Phase behavior and nanoscale structure of phospholipid membranes incorporated with acylated C_{14}-peptides, Biophys. J. 89 (2005) 2494–2503.
[20] V.D. Gordon, P.A. Beales, Z. Zhao, C. Blake, F.C. MacKintosh, P.D. Olmsted, M.E. Cates, S.U. Egelhaaf, W.C.K. Poon, Lipid organization and the morphology of solid-like domains in phase-separating binary lipid membranes, J. Phys. Condens. Matter 18 (2006) L415–L420.
[21] U. Bernchou, H. Midtiby, J.H. Ipsen, A.C. Simonsen, Correlation between the ripple phase and stripe domains in membranes, Biochim. Biophys. Acta 1808 (2011) 2849–2858.
[22] T. Heimburg, A model for the lipid pretransition: coupling of ripple formation with the chain-melting transition, Biophys. J. 78 (2000) 1154–1165.
[23] T. Kaasgaard, C. Leidy, J.H. Crowe, O.G. Mouritsen, K. Jorgensen, Temperature-controlled structure and kinetics of ripple phases in one- and two-component supported lipid bilayers, Biophys. J. 85 (2003) 350–360.
[24] F. Yarrow, B.W.M. Kuipers, AFM study of the thermotropic behaviour of supported DPPC bilayers with and without the model peptide WALP23, Chem. Phys. Lipids 164 (2011) 9–15.
[25] E.Y. Shalaev, P.L. Steponkus, Phase behavior and glass transition of 1,2-dioleoylphosphatidylethanolamine (DOPE) dehydrated in the presence of sucrose, Biochim. Biophys. Acta 1514 (2001) 100–116.
[26] K. Jorgensen, O.G. Mouritsen, Phase separation dynamics and lateral organization of two-component lipid membranes, Biophys. J. 95 (1995) 942–954.
[27] A.E. Regelin, S. Fankhaenel, L. Gurtesch, C. Prinz, G.V. Kiedrowsk, U. Massing, Biophysical and lipofection studies of DOTAP analogs, Biochim. Biophys. Acta 1464 (2000) 151–164.
[28] G.M.D. Gregorio, P. Mariani, Rigidity and spontaneous curvature of lipidic monolayers in the presence of trehalose: a measurement in the DOPE inverted hexagonal phase, Eur. Biophys. J. 34 (2005) 67–81.
[29] S.J. Kim, H.H. An, S.J. Lee, J.H. Lee, Y.H. Kim, C.S. Yoon, S.H. Suh, Formation of Ag nanostrings induced by lyotropic liquid crystalline phospholipid multilayer, Langmuir 28 (2012) 259–263.